International Journal of Thermal Sciences 49 (2010) 543–554

Contents lists available at ScienceDirect

International Journal of Thermal Sciences

journal homepage: www.elsevier.com/locate/ijts

Experimental study of the emissivity of flames resulting from the combustion of forest fuels

A. Àgueda, E. Pastor, Y. Pérez, E. Planas*

Centre d'Estudis del Risc Tecnològic (CERTEC), Universitat Politècnica de Catalunya, ETSEIB, Diagonal 647, pav. G, planta 2, 08028 Barcelona, Catalonia, Spain

ARTICLE INFO

Article history:
Received 19 January 2009
Received in revised form
25 June 2009
Accepted 25 September 2009
Available online 12 October 2009

Keywords:
Extinction coefficient
Flame transmissivity
Forest fires
Heat flux transducer
Infrared thermography
Long-term retardants
Radiation

ABSTRACT

Heat transfer by radiation is taken into account in most models that predict the propagation of forest fires. This heat transfer mechanism is normally formulated according to the Stefan–Boltzmann law in terms of flame temperature and flame emissivity. This study focused on flame emissivity. Experimental studies carried out to compute the emissivity of the flames generated during the combustion of forest fuels were reviewed, thereby highlighting differences in methodologies and results. Since the results of these studies with regard to the exponential relationship between flame emissivity and flame thickness were not in agreement, two methods based on IR imagery were used in the present study to calculate flame emissivity values. Nine circular fuel beds with a diameter of 0.3–2.5 m were prepared with common Mediterranean species and burned as stationary fires. An exponential correlation between flame emissivity and flame thickness was observed for both methods. According to the results of this study, only flames thicker than 3.2 m would exhibit an emissivity close to that of a blackbody (0.9), and the associated extinction coefficient would be 0.72. A long-term retardant product was used to treat the fuel of two of the nine tests that were carried out and no effect on flame emissivity was observed.

1. Introduction

Thermal radiation is one of the three types of heat transfer responsible for forest fire propagation, together with convection and conduction. Heat transfer by radiation has been taken into account to predict propagation in most forest fire models [1,2]. It is known to be the dominant mechanism in cases where a flame front propagates in a homogeneous horizontal fuel bed in the absence of wind [3]. However, the role of the various heat transfer mechanisms in forest fire propagation is being further investigated for other forest fuel bed configurations, i.e. considering slope, or ambient conditions, such as the presence of wind [4–6].

In complete theoretical models for forest fires propagation, extinction coefficient and radiative intensity associated to the flame are necessary parameters to solve the radiative transfer equation [2]. However, flame emissivity is a required parameter in simplified theoretical models [1]. In this last type of models, heat transfer by radiation is normally formulated according to the Stefan–Boltzmann law in terms of flame temperature and emissivity, and by considering the view factor between the flame and the fuel ahead of the flame front. Flame temperature and emissivity cannot easily be evaluated experimentally because flames generated during forest fires are heterogeneous and turbulent, and most authors assume an isothermal flame surface with a certain emissivity [7] or use emissive power data to handle with radiation [8,9].

A few experimental studies have used various methods to measure the emissivity of forest fuel flames. Most of the authors of these studies have based their work on the assumption that emissivity values can be given for a kind of equivalent medium. Most of these studies have found emissivity values to be related to flame thickness, but there is disagreement on the results of the coefficient relating these two variables, i.e. the extinction coefficient. Furthermore, recent years have seen an increase in the use of infrared (IR) cameras in applications related to forest fires. IR systems behave like a heat flux transducer formed by a two-dimensional array of sensors and can transform signals from the sensors into temperatures by specifying the ambient temperature, relative humidity, distance and emissivity of the viewed object. Thus, quantitative thermal measurements made with IR cameras require a good estimate of the emissivity of the object under study (that is, the flame or the burning fuel bed, in forest fire applications). Moreover, most comprehensive studies were done before the 1980s, at a time when IR imaging systems were not commonly used in applications related to forest fires. This study takes advantage of the spatial resolution of the IR cameras to compute the emissivity of forest fuel flames.

* Corresponding author. Tel.: +34 934016675; fax: +34 934017150.
E-mail address: eulalia.planas@upc.edu (E. Planas).

1290-0729/$ – see front matter © 2009 Elsevier Masson SAS. All rights reserved.
doi:10.1016/j.ijthermalsci.2009.09.006

Nomenclature

$bb1$	Blackbody 1
$bb2$	Blackbody 2
F_f	View factor between the flame and the transducer according to Eq. (5)
$F_{(i,j)k}$	View factor between the cell (i,j) of the k-th image of the IR sequence and the heat flux transducer (−)
i	Rows of the temperature matrix (from 1 to 240)
I_0	Radiation intensity at the origin of the radiation path (W m^{-2})
I_{bb1}	Radiation emitted by $bb1$ in the absence of flame (W m^{-2})
I_{bb2}	Radiation emitted by $bb2$ in the absence of flame (W m^{-2})
I_f	Radiation intensity of the flame according to Eqs. (6)–(8) (W m^{-2})
I_{f+bb1}	Radiation emitted by the flame plus the part of radiation emitted by $bb1$ that is transmitted by the flame (W m^{-2})
I_{f+bb2}	Radiation emitted by the flame plus the part of radiation emitted by $bb2$ that is transmitted by the flame (W m^{-2})
I_δ	Radiation intensity at the end of the radiation path (W m^{-2})
j	Columns of the temperature matrix (from 1 to 320)
k	Number of the image of the IR sequence
m	Columns of the study area (from 1 to 10)
n	Rows of the study area (from 1 to 10)
P	Row of the temperature matrix at the interface between the flame and the fuel bed
OS	Object signal
$OS_{bb673_{(n,m)}}$	OS mean value associated with the (n,m) element of the study area limited by the radiating panel at 673 K in the absence of flame
$OS_{bb573_{(n,m)}}$	OS mean value associated with the (n,m) element of the study area limited by the radiating panel at 573 K in the absence of flame
$OS_{f+bb673_{(n,m)k}}$	OS mean value associated with the (n,m) element of the study area limited by the radiating panel at 673 K for the k-th image of the IR sequence
$OS_{f+bb573_{(n,m)k}}$	OS mean value associated with the (n,m) element of the study area limited by the radiating panel at 573 K for the k-th image of the IR sequence
q''_{rt}	Radiation heat flux received by the transducer (W m^{-2})
T_f	Flame temperature according to Eqs. (4)–(6) (K)
$T_{(i,j)k}$	Temperature of the cell (i,j) of the k-th image of the IR sequence (K)
$(V_{bb})_{T=T_f}$	Radiometer output for blackbody source at flame temperature (V)
V_f	Radiometer output for flame radiation (V)

Greek symbols

α_f	Absorptivity of the flame (−)
δ	Radiation path (m)
δ_f	Flame thickness (m)
δ_{f_m}	Mean flame thickness (m)
$\delta_{f_{rp}}$	Thickness of the flame at the region covered by the radiating panels (m)
κ	Extinction coefficient (−)
κ_f	Flame extinction coefficient (−)
ε_b	Emissivity of the burning fuel (−)
ε_f	Flame emissivity (−)
$\varepsilon_{(n,m)k}$	Emissivity associated with the (n,m) element of the k-th image of the IR sequence (−)
σ	Stefan–Boltzmann constant (5.67 × 10^{-8} W m^{-2} K^{-4})
τ_a	Atmospheric transmissivity (−)
τ_f	Flame transmissivity (−)

The first specific aim of this study was to review experimental methods used up to the present time to compute flame emissivity, and to analyze their differences and results. Based on this review, a second specific aim was defined: to apply two different IR-based methods to compute flame emissivity, to compare the results with those presented in the literature, and to examine the types of results obtained by the two methods. The first method (Method 1) is based on the measurement of flame transmissivity. The second one (Method 2) is based on the use of heat flux data obtained by a transducer. The third specific aim was to improve knowledge of the relationship between the emissivity and thickness of a flame by studying a range of thicknesses (greater than 2 m) that were wider than those covered in other studies. The last specific aim was to determine whether the presence of an ammonium-polyphosphate-based retardant product could have some effect on flame emissivity.

The hypothesis guiding this last specific aim was that differences might be observed in flame emissivity values, since concentrations had increased for some gaseous products (H_2O, NH_3, etc.) generated during the combustion of forest fuels that had previously been treated with long-term retardants [10,11]. As noted by King [12], high concentrations of water can have a great influence on flame emissivity. Moreover, because ammonia has absorption bands within the IR range, the presence of this compound could modify the spectral distribution of the radiant energy from the flames [13].

The medium which is of interest here, forest fuel flames, is heterogeneous (temporarily and locally). However, results presented in this study have been obtained for a kind of equivalent medium with average radiative properties. Since the main objective of this study was to compute emissivity values by using two different methods, this simplification had to be undertaken to be able to compare them.

1.1. Background on forest fuel flames

Flames generated during the combustion of forest fuels are turbulent, diffusive and very luminous. They emit energy in the visible and IR regions of the electromagnetic spectrum. The emitted radiation comes from both hot gases (basically CO_2 and H_2O vapour, and also CO) and solid particles of incandescent soot. Gases present in the flame have discrete absorption bands in the IR spectrum. The maximums for CO_2 are at 2.7, 4.4 and 15 μm; for H_2O they are at 1.4, 1.9, 2.7, 6 and 17 μm. Soot particles emit radiation in a continuous spectrum over a wider region from the visible to the IR. The more the wavelength increases, the greater the drop in emissivity [14]. Nevertheless, this reduction in emissivity is disregarded by most authors [15] and soot particles are considered to behave as grey bodies (i.e. absorptivity is independent of wavelength and temperature). Hägglund and Persson [16] estimated the relative contribution of soot radiation and band radiation (associated to hot gases) at different flame thicknesses. They obtained that for thin flames (<0.20 m) band radiation dominated, whereas the contribution of soot radiation to flame radiation dominated with increasing flame thickness.

Radiation originates throughout the flame and travels through the atmosphere before being captured by an object (e.g. fuel, a firefighter, a sensor, etc.). Since the atmosphere contains CO_2 and H_2O vapour, in some regions of the electromagnetic spectrum the atmosphere absorbs to some degree the IR radiation of these gases. These regions contrast with others, known as atmospheric windows, where the atmosphere is almost transparent and high atmospheric transmissivity is assured. The most important windows are the visible/near IR region (from 0.4 to 2.5 μm), the middle IR region (from 3 to 5 μm) and the thermal IR region (from 8 to 12 μm). In the most recent studies, the sensors used to compute flame emissivity operate in the thermal IR region. In this spectral range, the CO_2 and the H_2O vapour make a small contribution to the radiation and the emission of radiant energy is dominated by soot [17].

The radiation properties of soot are usually described by the Mie theory, which applies to the polydispersion of spherical particles. According to this theory, if the diameter of the particles is small with respect to the wavelength (Rayleigh limit), then the radiation scattering coefficient is negligible. Since the diameter of soot particles generated during the combustion of forest fuels normally ranges from 0.02 to 0.7 μm [17], in the thermal IR range, it can be assumed that the Rayleigh limit is valid and the reflectivity of the flame is zero. The emissivity of the flame is given by Eq. (1) if it is assumed that Kirchoff's law holds for soot particles in the spectral range of the camera. According to this law, at thermal equilibrium, the emissivity of a flame is equal to its absorptivity.

$$\varepsilon_f = \alpha_f = 1 - \tau_f \tag{1}$$

According to Eq. (1), forest fuel flames constitute a medium that absorbs and transmits radiation. Bouguer's law (see Eq. (2)) states that radiation intensity along a path is attenuated exponentially while it passes through an absorbing medium. If the medium is uniform, the exponent is equal to the product of the path length traversed (δ) and a coefficient known as the extinction coefficient (κ).

$$I_\delta = I_0 \exp(-\kappa\delta) \tag{2}$$

Using Eq. (1), this equation can be rewritten to obtain an expression (Eq. (3)) for the emissivity of the flame that depends on the extinction coefficient and the length of the absorbing path (in this case, flame thickness).

$$\varepsilon_f = 1 - \exp(-\kappa_f \delta_f) \tag{3}$$

2. Review of experimental methods

Since 1971, several authors have performed experimental studies to determine the emissivity of flames generated during the combustion of forest fuels. The earliest studies used heat flux transducers (HFT), spectrophotometers (SPH) and thermocouples (TC), whereas the most recent studies used IR systems.

In the earliest studies, several authors burned either *Picea excelsa* cribs or heather and gorse fuel beds in stationary and propagating fires, respectively. The maximum measured flame temperature was 1353 K and the maximum estimated flame emissivity was 0.94 for flame thicknesses of 2 m. Table 1 shows other relevant experimental characteristics and results. Each study used a different method to compute flame emissivity. Beyreis et al. [18] determined flame emissivity with an HFT and a thermocouple. HFT outputs (in voltage units) were directly used to compute flame emissivity because they used the same geometric arrangement of the radiating source and the HFT in the calibration of the HFT with a blackbody and in the experiments. The quotient between the HFT output for flame radiation and for the blackbody source at flame temperature gave an emissivity value (see Eq. (4)).

$$\varepsilon_f = \frac{V_f}{(V_{bb})_{T=T_f}} \tag{4}$$

Thomas [19] determined the emissivity of tilted flames of propagating fire fronts. He measured flame temperatures with thermocouples and flame irradiance with an HFT. He used the Stefan–Boltzmann law to quantify the emissive power of the flames, assumed an atmospheric transmissivity equal to 1 and calculated the view factor between the flame and the HFT to obtain an emissivity value (see Eq. (5)).

$$\varepsilon_f = \frac{q''_{rt}}{\sigma T_f^4 F_f} \tag{5}$$

Thomas obtained low emissivity values. This can be explained by the more efficient combustion in the flame resulting from the increased air entrainment due to wind. In this study, a slightly modified version of this author's approach was used to compute flame emissivity according to Method 2.

Some years later, Hägglund and Persson [16] computed flame emissivity from radiant spectral intensity data obtained with a spectrophotometer in the 1–5.5 μm range. They integrated spectral intensity curves to obtain the radiation intensity of the flame (I_f) and assumed a somewhat arbitrary flame temperature of 1300 K to solve Eq. (6).

$$\varepsilon_f = \frac{I_f}{\sigma T_f^4} \tag{6}$$

In a recent study [20], irradiation measures obtained with two HFTs were used to compute a mean extinction coefficient of a simulated flame front. This approach was clearly aimed at simulating flame fronts typical of forest fires, but the authors used propane as fuel to obtain experimental data. They represented the flame as a triangular prism with a constant temperature.

In recent studies, IR systems have been used to calculate flame emissivity. The relationship shown in Eq. (1) has been used in all studies to deduce an emissivity value from flame transmissivity.

The emissivity of a flame can be estimated by measuring the fraction of energy transmitted by the flame that comes from a body of known emissivity at a given temperature. More precisely, Eq. (7) can be written if a flame of unknown transmissivity is placed between a body of known emissivity (in this case, equal to 1) and an IR camera. The energy emitted by the flame (I_f) and the energy transmitted from the blackbody placed behind it ($\tau_f I_{bb1}$) are partial contributions of radiation with respect to the total radiation captured by the IR camera (I_{f+bb1}). An analogous equation can be written for a blackbody at another temperature (Eq. (8)) assuming an identical flame transmissivity. Nevertheless, as the incident radiation varies for the two blackbodies, theoretically so does the total transmissivity. This effect is assumed to be less important when blackbody temperatures are close. By combining the two equations, in accordance with Eq. (1) an expression for flame emissivity can be obtained (see Eq. (9)).

$$I_{f+bb1} = I_f + \tau_f I_{bb1} \tag{7}$$

$$I_{f+bb2} = I_f + \tau_f I_{bb2} \tag{8}$$

$$\varepsilon_f = 1 - \frac{(I_{f+bb2} - I_{f+bb1})}{(I_{bb2} - I_{bb1})} \tag{9}$$

The total radiation emitted by a flame cannot be accurately measured with an IR camera because this device is only sensitive in a specific region of the electromagnetic spectrum. However, if it is

Table 1
Main experimental characteristics and results of the methods developed to measure the emissivity of the flames generated during the combustion of forest fuels with heat flux transducers (HFT), spectrophotometers (SPH) and thermocouples (TC) (n.s.: unspecified parameter; δ_f: flame thickness; T_f: flame temperature; ε_f: flame emissivity; κ_f: flame extinction coefficient).

Reference	Number of tests	Fuel	Fuel beds dimensions (m)			Equipment			Results			
			Height	Width	Depth	Flame radiant intensity	Flame thickness	Flame temperature	δ_f (m)	T_f (K)	ε_f (−)	κ_f (m^{-1})
[18]	5	*Picea excelsa* cribs	0.76	1.14–1.52	0.38–1.91	HFT	Lateral visual observations	TC	0.27–1.88	644–1289	0.11–0.66	0.51
[19] [a]	7	Heather and gorse fuel beds	0.35–1.50	n.s.	n.s.	HFT	Photographs	TC	0.80–3.00 (base of the flame)	1253–1353	0.06–0.47	0.10
[16]	16	*Picea excelsa* cribs	n.s.	1.20	n.s.	SPH (1–5.5 μm)	Lateral visual observations	TC	0.15–2.00	873–1303	0.12–0.94	1.03

[a] Tilted flame front.

assumed that forest fuel flames behave like grey bodies, it is not necessary to know the total radiation emitted by the flame in order to apply Eq. (9) because radiation measurements determined within a specific range are compared with each other.

In this study, this methodology is referred to as the 'flame transmission method'. It was applied to compute flame emissivity in Method 1. More details about the theoretical deduction of Eq. (9) are given in [17].

Only three experimental studies carried out with forest fuels have computed flame emissivity using the flame transmission method. Table 2 shows their main experimental characteristics, as well as the emissivity ranges obtained. The main difference between these studies lies in the number, arrangement and temperature of the blackbodies that were used. The studies of Den Breejen et al. [21] and Pastor et al. [22] used just one blackbody (*bb*1). In fact, measurements relative to the *bb*2 blackbody in Eq. (9) were taken with the background behind the flame. In the study of Den Breejen et al. [21], a chopper placed in front of the *bb*1 blackbody was quickly opened and closed. When the chopper was closed, only background radiation remained. The *bb*1 blackbody had a temperature of 900 K. Pastor et al. [22] assumed a symmetric flame and placed the *bb*1 blackbody (at ambient temperature) on one side of the two halves that vertically divided the flame. Dupuy et al. [17] used three blackbodies. Two of them were radiating at the same temperature (ambient temperature) and their mean radiation intensity was used as data for the blackbody *bb*1. The other blackbody (*bb*2) had a temperature of 523 K. Fig. 1 shows the position of the blackbodies that were used in these studies. A common characteristic of these three works was that experimental data were obtained in a specific wavelength or spectral range. If it is assumed that flames are dominated by soot and that soot emissivity is not dependent on wavelength, this is not a problem but, according to the results of [16], this is only true if flame thickness is greater than 0.20 m. According to Table 2, this condition was only probably fulfilled by flames in [22]. For this reason, the authors of the study [17] may have computed total properties for soot. They calculated gas emissivities to correct the values of measured transmittance for soot contribution only, and then computed the contribution of soot to the total extinction coefficient (see [17] for more details). This approach was not followed in this study on the assumption that flames were soot dominated. In the results and discussion section this assumption is commented.

3. Experimental methods

In this study, experiments with static fires were carried out under laboratory and field conditions. Four tests were performed in the laboratory and five tests in the field. Two of the laboratory tests used Method 1, while the other two used Method 2. In the field experiments, both methods were applied in all of the tests. Laboratory tests were replicated one time. Most field tests were carried out only once due to performance difficulties associated with this type of fires and the variability of the test conditions, in terms of wind, temperature and relative humidity. Only field tests performed with retardant-treated fuel could be replicated.

3.1. Tests conditions

Four common Mediterranean species were used as fuel to be burned. *Pinus halepensis* needles were used in the laboratory tests. The field tests used branches and dead leaves of three species: *Erica arborea*, *Quercus ilex* and *Quercus humilis*. Only fuel with a diameter of less than 15 mm was used in the field tests. Different fuels had to be used due to availability constraints. The use of different fuel could limit comparison between laboratory and field tests. However, distinctions between species were not considered when analyzing the experimental results on the assumption that flames composition of burning fine forest fuels was similar regardless of

Table 2
Main experimental characteristics and results of the methods developed to measure the emissivity of the flames generated during the combustion of forest fuels with IR systems (n.s.: unspecified parameter; H: height; W: width; *bb*1: blackbody 1; *bb*2: blackbody 2; δ_f: flame thickness; ε_f: flame emissivity; κ_f: flame extinction coefficient).

Reference	Number of tests	Spectral range (μm)	Fuel	Characteristic length of the fuel bed (m)	Blackbody dimensions (H × W; m)	Temperature of *bb*1 (K)	Temperature of *bb*2 (K)	Results		
								δ_f (m)	ε_f (−)	κ_f (m^{-1})
[21]	n.s.	5, 10	n.s.	0.08 (diameter)	*bb*1: n.s.	900	–	n.s.	0.23–0.40	n.s.
[22]	4	7.5–13	*Pinus halepensis* needles and fine branches *Rosmarinus officinalis* branches	0.25, 0.50, 1.00 (side of a square)	*bb*1: 0.8 × 0.4	Ambient temperature	–	0.25, 0.50, 1.00[b]	0.55–0.83	3.11, 2.24
[17]	45	7.5–13	*Pinus pinaster* needles	0.20, 0.28, 0.40 (diameter)	*bb*1: n.s.[a] *bb*2: 0.1 × 0.1	Ambient temperature	523	0.11–0.23	0.02–0.28 (0.10–0.55[c])	n.s. (0.70–6.20[c])

[a] Two *bb*1 blackbodies.
[b] Side of the fuel bed.
[c] For soot at the complete spectral range.

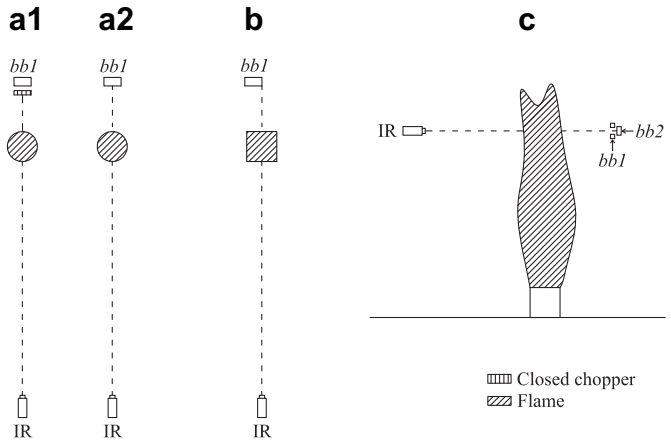

Fig. 1. Outline of the transmission devices used in: (a) Den Breejen et al. (1998) [21] (a1 sketches a time instant in which the chopper was closed and a2 sketches a time instant in which the chopper was opened) (top view); (b) Pastor et al. (2002) [22] (top view); and (c) Dupuy et al. (2007) [17] (lateral view) (*bb*1: blackbody 1; *bb*2: blackbody 2; IR: infrared camera).

the small differences in chemical constitution and surface area to volume ratios.

Circular fuel beds were arranged and burned. The ones prepared in the laboratory had a mean diameter of 0.35 m, while those prepared in the field had a diameter of 2.5 m. The mean bulk density of the fuel beds was 22 and 10 kg m^{-3} for laboratory and field tests, respectively. Table 3 shows the specific values corresponding to each test.

The mean ambient conditions for the laboratory tests were an ambient temperature of 290 K and a relative humidity of 45%. Before the experiments, the pine needles were dried in an oven at 353 K for 24 h. The mean ambient conditions for the field experiments were an ambient temperature of 283 K and a relative humidity of 63%. In these tests, the mean fuel moisture was 12.5% (SD 3.7%). Differences in fuel moisture content were not considered in the analysis of the experimental results because, according to the results of King [12], this variable can only change emissivity values significantly at values greater than 20%.

The fuel used in the field tests EA ret1 and EA ret2 (see Table 3) was previously treated with a commercial long-term retardant product called Fire-Trol 931, which is ammonium-polyphosphate based. For each kg of fuel, a 0.75 l dilution of the product with water (15% V/V) was applied. Before the burnings, the water of the dilution was evaporated. According to Vélez [23], a coverage level of 1 l m^{-2} is commonly applied on fuel models 4, 5 and 6 [24], which are typical of the Mediterranean basin. The ratio used in this study is equivalent to the mean value that would be obtained if the same product dilution was applied to the aforementioned fuel models.

Different methods were used to ignite the fuel beds in each type of test. In the laboratory, ignition was carried out by placing under the fuel bed a circular receptacle containing alcohol which was removed after complete ignition of the base of the fuel bed. It was possible to perform this kind of ignition because the fuel bed was placed on a wire netting 0.2 m above the ground. With this type of ignition, the fuel bed was completely ignited almost instantaneously. In the field, the fuel bed was placed on the ground and ignition was done on the top surface. Two people carried out a homogeneous ignition with drip torches. Due to the dimensions of the fuel bed, combustion propagated downwards through it during the test.

3.2. Experimental set-ups

3.2.1. Method 1

The devices needed to compute flame emissivity according to Method 1 were an IR camera and two hot blackbodies. Qian and Saito [25], who worked with hydrocarbons, also used two hot blackbodies to compute emissivity values for hexane flames. The blackbodies used in this study were placed on either side of the vertical axis of symmetry of the bed, one next to the other. Fig. 2(a) and (c) show the arrangement of the blackbodies with respect to the IR camera for laboratory and field experiments, respectively. There was a distance of 0.4 and 0.6 m between the base of the radiating panels and the base of the fuel beds in the laboratory and field tests, respectively.

Two black-colored radiating panels (0.5 m tall, 0.3 m wide) were used to simulate the blackbodies. They were heated to temperatures of around 573 K and 673 K. The temperatures were regulated by a PID controller that considered the value measured by a thermocouple (type J; 0.3 cm in diameter) placed in the middle of the panel. The set temperatures allowed us to work in the medium and high brightness temperature ranges of the IR camera (see Table 4) because the IR camera can, in fact, measure brightness temperatures outside of the ranges indicated by the manufacturer. For example, in the high range, the camera can measure brightness temperatures starting at around 500 K.

The IR camera that was used (AGEMA Thermovision 570-Pro) operates at the thermal IR window. Table 4 specifies its main technical characteristics. IR image sequences were recorded in the medium and high brightness temperature range in laboratory and

Table 3
Main characteristics of the experimental tests: bulk density and dimensions of fuel bed, and flame thickness (D: diameter; H: height; δ_{f_m}: mean flame thickness; $\delta_{f_{rp}}$: thickness of the flame in the region vertically covered by the radiating panels; SD: standard deviation).

Test type	Test name	Forest species	Fuel bed bulk density (kg m^{-3})	Fuel bed dimensions (D × H; m)	δ_{f_m} (SD) (m)	$\delta_{f_{rp}}$ (SD) (m)
Laboratory	PH1	*Pinus halepensis*	19.9	0.30 × 0.20	–	0.24 (0.06)
	PH2		21.5	0.30 × 0.20	–	0.28 (0.06)
	PH3[a]		22.9	0.40 × 0.20	0.27 (0.09)	–
	PH4[a]		22.8	0.40 × 0.20	0.25 (0.17)	–
Field	EA	*Erica arborea*	10.6	2.50 × 0.70	2.28 (0.54)	2.28 (0.12)
	EA ret1[b]		10.2	2.50 × 0.70	1.10 (0.44)	1.35 (0.25)
	EA ret2[b]		9.7	2.50 × 0.73	1.77 (0.34)	1.97 (0.10)
	QI	*Quercus ilex*	10.3	2.50 × 0.70	1.00 (0.51)	1.40 (0.20)
	QH	*Quercus humilis*	8.8	2.50 × 0.60	1.52 (0.78)	1.32 (0.06)

[a] Test without radiating panels.
[b] Fuel treated with a commercial long-term retardant product.

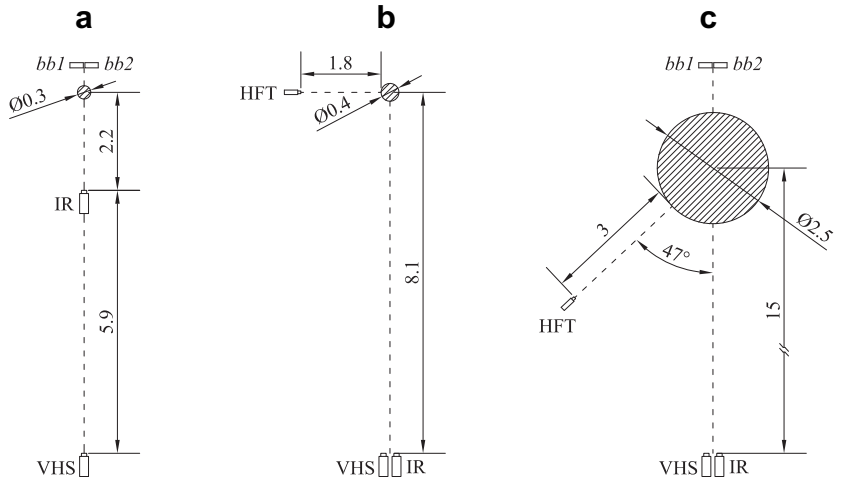

Fig. 2. Outline of the experimental set-ups used in this study (top view): (a) Laboratory tests, Method 1; (b) Laboratory tests, Method 2; (c) Field tests, Method 1 and Method 2. Patterns of inclined lines are associated with flame. Units are in m.

field tests, respectively. A conventional digital VHS camera (Sony Handycam Vision CCD-TR840E), which records visible light, was also used to film the experiments. In the field tests, the IR and VHS cameras were placed side by side (see Fig. 2(c)). The distance between the fire and the cameras (15 m) was such that the entire flame was visible. In the laboratory tests, however, the distance between the fire and the IR camera (2.2 m) was such that only the area between the two radiating panels was visible. The flame was only viewed in its entirety by the VHS camera, which was placed 8.1 m from the center of the fuel bed (see Fig. 2(a)).

3.2.2. Method 2

The devices needed to compute flame emissivity according to Method 2 were a heat flux transducer (HFT) and an IR camera. A VHS camera was also used to record the evolution of the flame. The HFT used in this work (Medtherm, Schmidt-Boelter thermopile, 64-2-16) has a recording frequency of 2 Hz and its working range is from 0 to 23 kW m^{-2}. The cameras were the same ones mentioned in the previous subsection.

The position of the HFT varied depending on the type of test. In the laboratory, it was placed 2 m from the center of the fuel bed, forming a right angle with the line defined by the IR camera and the center of the fuel bed (x-axis), and 0.38 m above the base of the fuel bed. In field tests, the HFT was placed 4.25 m from the center of the fuel bed, forming an angle of 47° with the x-axis, at a height of 1.34 m. Fig. 2(b) and (c) show the position of this device. The HFT was placed at an angle to the x-axis in order to prevent its shape from blocking part of the flame in the recorded images. In the field tests, this position made it possible to disregard the contribution of the radiating panels to irradiance, because their view factor was negligible with respect to that of the flame.

Table 4
Technical specifications of the AGEMA 570 camera.

Field of view	24° × 18°
Thermal sensitivity	<0.15 K
Image frequency	4 Hz
Detector type	Focal plane array (FPA), uncooled microbolometer, 320 × 240 pixels
Spectral range	7.5–13 μm
Brightness temperature measurement ranges	Low: 253–393 K/Medium: 353–773 K/High: 623–1773 K
Measurement accuracy	±2°

The tests were recorded with both the IR camera and the VHS camera. The distance between the cameras, placed side by side, and the fire was such that the entire flame was visible. They were placed 8.1 m and 15 m from the center of the fuel bed in the laboratory and field tests, respectively (see Fig. 2(b) and (c)). IR image sequences were recorded in the camera's high brightness temperature range.

4. Calculation methods

4.1. Flame emissivity

4.1.1. Method 1

This method applies the flame transmission method using the set-up described above. The application of this method is limited to flames that present geometric and thermodynamic symmetry with respect to the radiating panels. From a practical point of view, 'geometric symmetry' means that the tilt angle of the flame is zero. The thermodynamic characteristics of a flame (e.g. composition, temperature, etc.) have to be similar with respect to both radiating panels in order for a flame to be completely symmetric. In order to meet the condition of geometric symmetry, each test was studied only in a time domain in which the tilt angle of the flame was practically zero (±5° and ±15° for laboratory and field experiments, respectively). An algorithm developed with MATLAB [26] was used to determine the tilt angle of the flame as a function of time. Images recorded with the VHS camera were used to obtain this angle. The condition of thermodynamic symmetry was assumed to be met.

IR image sequences recorded in the presence of the radiating panels were used to apply Method 1. Calculations were performed using an output unit of the IR camera that is proportional to the amount of radiation sensed by the camera detector, the Object Signal (OS) unit.

For each image of the time domain selected for each test, the OS values of the pixels inside the areas limited by the radiating panels were extracted. Two 10-by-10 matrices were created (see Fig. 3) and each of their elements contained the mean OS value of the corresponding pixels ($OS_{f+bb673_{(n,m)k}}$ and $OS_{f+bb573_{(n,m)k}}$). In the laboratory tests, around 130 pixels were considered in order to compute the mean OS value of each element of the matrices. In the field tests, since the distance between the radiating panels and the fuel bed was greater, only around two pixels were considered. The area of each element of the matrices represented 15 cm^2. The area occupied by the radiating panels was divided into 100 subareas in order

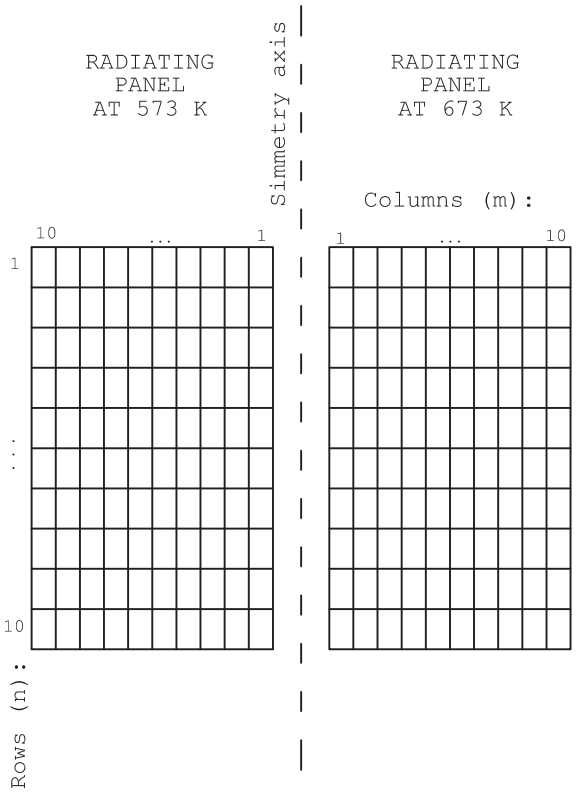

Fig. 3. Splitting of the study area into two 10-by-10 matrices for flame emissivity calculation according to Method 1.

to restrict the study to those subareas covered by the flame and also to observe whether there were any spatial trends within the flame.

The same procedure was followed for an IR image of the beginning of the sequence in which only the radiating panels were present, without flame in front of them. The OS values of the elements of the radiating panels were determined ($OS_{bb673_{(n,m)}}$ and $OS_{bb573_{(n,m)}}$) and considered to be constant for each test. Eq. (10), which is analogous to Eq. (9), was applied to each pair of elements (n,m) of the matrices in order to obtain an emissivity value for each pair of elements at each time instant k.

$$\varepsilon_{(n,m)k} = 1 - \frac{\left(OS_{f+bb673_{(n,m)k}} - OS_{f+bb573_{(n,m)k}}\right)}{\left(OS_{bb673_{(n,m)}} - OS_{bb573_{(n,m)}}\right)} \tag{10}$$

The emissivity value for each test, which is associated with the flame in the chosen time domain and in the area limited by the radiating panels, was computed as the median of all physically valid emissivity values (between 0 and 1) of the elements of the matrices in which there was flame. The median estimate was used because this measure is resistant to outliers, which were mainly observed in laboratory tests.

4.1.2. Method 2

In Method 2, heat flux data recorded with the HFT and image sequences recorded with the IR camera were used to obtain a mean emissivity value of the flame.

The time domain used in Method 2 was the same as the one used in Method 1 for field tests. In laboratory tests, it was fixed according to the same criterion used in Method 1.

The heat flux captured by the HFT was considered to be coming from the thermal radiation of the fire, which had two different sources: the flame and the fuel bed burning with glowing combustion. Since the distance between the IR camera and the fire was high, the fire was considered to be an imaginary wall that showed the apparent temperature distribution obtained by the IR camera and was placed perpendicular to the HFT. The temperature of each element of the wall, i.e. each pixel in the IR image, was transformed into emissive power using the general case of the Stefan–Boltzmann law (i.e. for a grey body characterized by a given emissivity). Afterwards, emissive power values were transformed into irradiance by considering the atmospheric transmissivity and the view factor between each element of the imaginary wall and the HFT. Eq. (11) expresses the corresponding energy balance.

$$\begin{aligned} q''_{rt} = {} & \varepsilon_f \sigma \sum_{i=1}^{P} \sum_{j=1}^{320} \left[\left(T_{(i,j)k}(\varepsilon_f) \right)^4 \tau_a F_{(i,j)k} \right] \\ & + \varepsilon_b \sigma \sum_{i=P+1}^{240} \sum_{j=1}^{320} \left[\left(T_{(i,j)k}(\varepsilon_b) \right)^4 \tau_a F_{(i,j)k} \right] \end{aligned} \tag{11}$$

In this equation temperature terms $T_{(i,j)k}(\varepsilon_f)$ and $T_{(i,j)k}(\varepsilon_b)$ account for emissivity dependent temperatures.

The pixels row of IR images at the interface between the flame and the fuel bed (P) was visually estimated and fixed for each test. To distinguish the fire from its surroundings, the pixels of the IR images were marked as 'fire' pixels if their temperature was greater than a threshold value of 500 K, and as 'background' pixels otherwise. The chosen threshold corresponded to a value slightly higher than the minimum temperature sensed by the IR camera. View factors were computed only for fire pixels; background pixels were assumed to have a view factor value of zero. A differential receptor was considered to compute the view factors. It was located perpendicular to the imaginary wall at distances of 1.8 m and 3 m from the wall for the laboratory and field tests, respectively. The atmospheric transmissivity, determined using the specific model integrated in the IR camera, was around 0.98 in all of the tests. The explicit function form of the model was reserved by the camera manufacturer [27].

As indicated in Eq. (11), temperature values ($T_{(i,j)k}$) were implicitly dependent on the emissivity value introduced as an input parameter in the ThermaCAM™ Researcher 2001 software. For fire pixels belonging to the burning fuel bed, emissivity (ε_b) was assumed to be equal to 1 [28]. The emissivity of the fire pixels belonging to the flame (ε_f) was the unknown variable.

To solve Eq. (11), which was implicitly defined, a least-squares method was used. The first term on the right-hand side of Eq. (11) was obtained by considering different ε_f values. The summed square of the difference between the left- and the right-hand sides of Eq. (11) at each time instant k of the time domain was then minimized.

4.2. Flame thickness

Since an axisymmetric medium was assumed for emissivity estimations, the thickness of the flame along the line of sight of the cameras (x-axis) was expected to be the same as the thickness along the y-axis (perpendicular to the x-axis).

The thickness of the flame was obtained from VHS images. The contour of the flame was extracted by converting greyscale images into binary images based on a luminosity threshold value. The distance between each pair of pixels of the contour of the flame along the horizontal axis of the image (y-axis in real coordinates) was computed in pixel units and converted to meters.

The mean thickness of the flame was computed by considering, at each time instant of the time domain, the complete contour of the flame. This variable was named δ_{f_m}. The thickness of the flame in the region covered by the radiating panels was computed in the

Fig. 4. VHS image of an arbitrary time instant of the QI field test that shows the flame contour extracted to compute flame thickness. The red lines indicate the part of the flame vertically covered by the radiating panels. (For interpretation of the references to colour in this figure legend, the reader is referred to the web version of this article.)

same way as δ_{f_m} but only for this region and was named $\delta_{f_{rp}}$. As an example, Fig. 4 shows an image of the QI field test, together with the contour extracted for the flame. The two horizontal lines in the figure indicate the part of the flame contour used to compute $\delta_{f_{rp}}$.

5. Results and discussion

Fig. 5(a) and (b) show examples of the type of flames obtained in the laboratory and field tests, respectively. Fig. 5(a) shows that the laboratory fires had a non-luminous region just above the burning fuel bed (at the flame base). This was a fluctuating region in which the flow was laminar. It can be attributed to gaseous compounds that remained unburned and to the smoke that was formed. The transition to turbulence occurred just above this region. Since gases, rather than soot, were predominant in this region, the radiating panels were placed just above it. Such a region was not present in the field fires because the flame was thoroughly turbulent. Corlett [29] already mentioned the presence (or lack thereof) of this region in pool fires.

Tests performed in the laboratory had a mean duration of 60 s. Three different phases of flame behaviour could be distinguished: an ignition phase of 5–10 s, an almost steady-state combustion phase (pseudo-stationary phase) lasting around 35 s (the time domains selected for emissivity calculations were all within this phase), and a third phase, lasting about 15 s, of transient combustion, characterized by unstable flame behavior, flame extinguishment and significant release of smoke. Finally, there was an extinguishing phase characterized by the glowing combustion of the remaining fuel residue. The field fires lasted around 150 s and 225 s for untreated and retardant-treated fuel tests, respectively. It was possible to distinguish three phases of flame behavior in these tests, as well. For tests performed with untreated fuel, the following phases were observed: an ignition phase lasting 15–40 s, a pseudo-stationary combustion phase lasting around 55 s (the time domains selected for emissivity calculations were all within this phase), and a third phase, lasting about 70 s, of transient combustion, characterized by unstable flame behavior and flame extinguishment. The glowing combustion of the remaining fuel residue was also observed after flame extinguishment. The three phases could be seen in the HFT curves. For tests performed with treated fuel, the corresponding phases lasted 40–100 s, 60 s and 95 s. Fig. 6 shows HFT data from a laboratory test and a field test, as well as the corresponding phases.

Time domains of around 5–10 s were selected for each test following the criterion of a flame tilt of approximately zero.

Fig. 7 shows an example of the type of results obtained with Method 1. The data are from the QI field test. The figure shows the evolution of the emissivity values calculated for several elements of the matrices. The amount of data available decreased as the column number increased. This indicates that the assumption of thermodynamic symmetry was not completely fulfilled as the distance between the compared elements increased. Plots of the emissivity distribution within the area covered by the radiating panels were also extracted by applying Method 1. Fig. 8 shows contour plots of the emissivity distribution for a laboratory test and a field test. There was no particular trend in the distribution of the emissivity values,

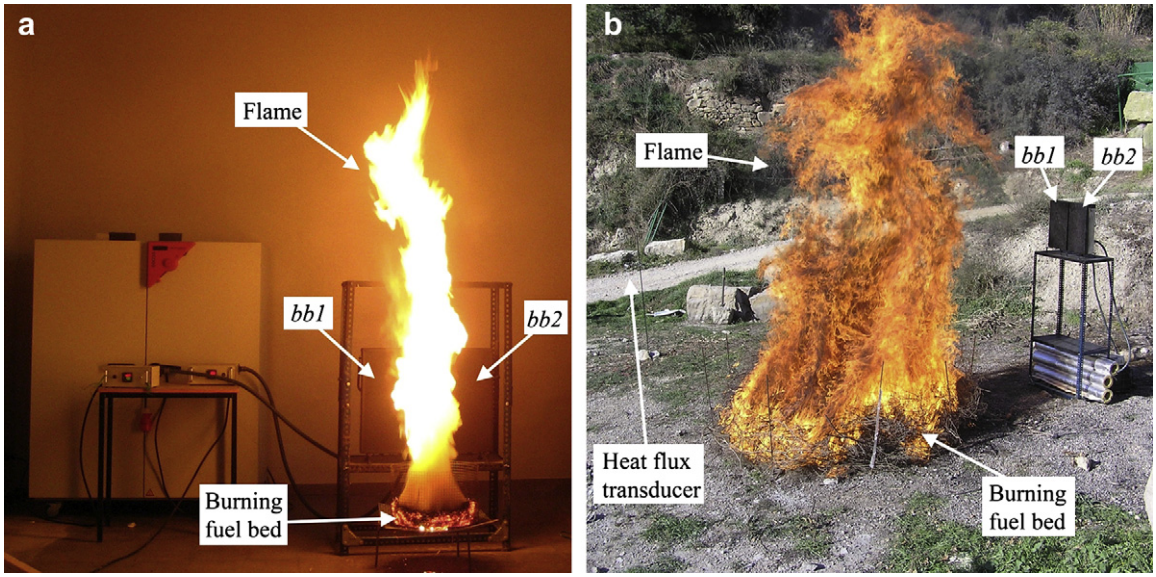

Fig. 5. Typical flames generated in experimental tests: (a) Laboratory fire; (b) Field fire. The devices, the flame and the burning fuel bed are indicated (*bb*1: blackbody 1; *bb*2: blackbody 2; HFT: heat flux transducer).

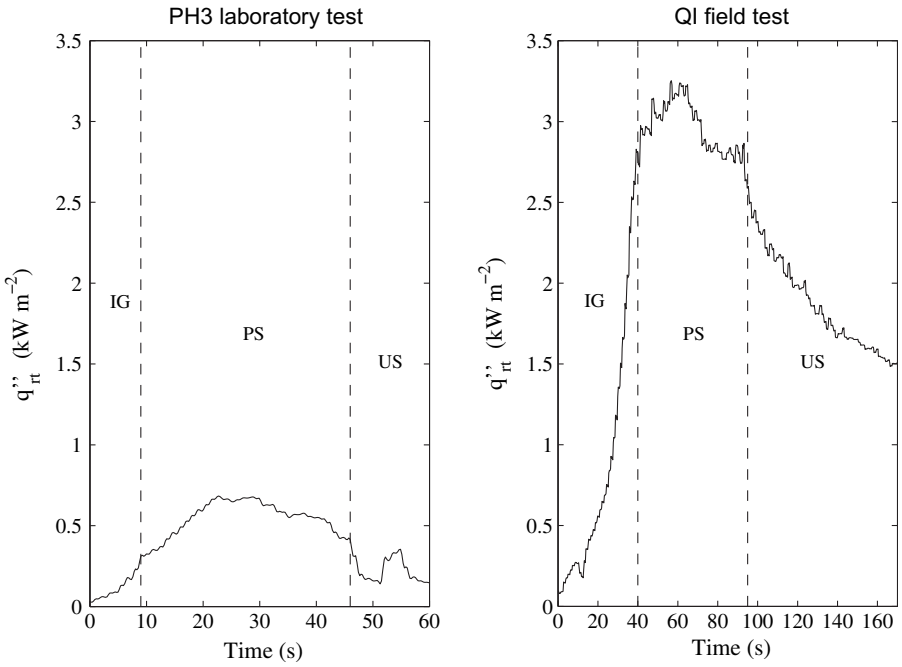

Fig. 6. Heat flux transducer data for a laboratory test and a field test. Phases of flame behavior are differentiated (IG: ignition; PS: pseudo-stationary; US: unstable).

but the contours were smaller and covered a wider range in the field test than in the laboratory test. This was probably due to a more turbulent flame. White regions of the plot indicate unavailable data. These regions were located either at the bottom or the right side of the contour plots. The unavailable data at the bottom of the plot are explained by the presence, before the fire, of branches blocking the view of the elements of the matrices representing the radiating panels. The unavailable data on the right side can be explained by the lack of symmetry between the associated elements, which led to the computation of invalid emissivity values.

Fig. 9 shows results corresponding to Method 2. The figure shows an example of the temperature values extracted from the IR images based on the emissivity value entered as an object's emissivity in the ThermaCAM™ Researcher 2001 software (ε_f or ε_b in Eq. (11)).

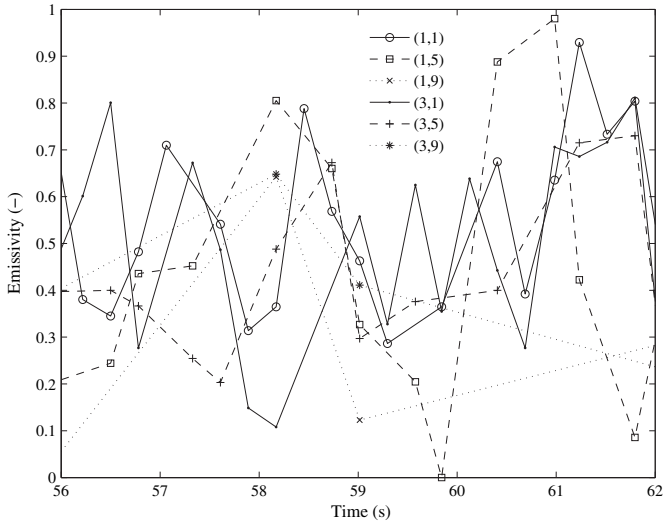

Fig. 7. Changes over time in the emissivity values associated with several elements of the matrices considered to compute flame emissivity according to Method 1. Element notation: (row, column).

The three images were taken at the same time instant during the PH3 laboratory test. The horizontal line represents the interface between the flame and the fuel bed. The results for three emissivity values (0.1, 0.2 and 1) are shown. Since flame temperatures are normally near 1100 K (see Table 1 or the results in [17]), based on the values displayed in Fig. 9, the flame emissivity associated with this test could be expected to be around 0.10–0.20. In fact, a value of 0.14 was computed for this test.

Fig. 10 shows flame emissivity values obtained by applying both Method 1 and Method 2 and taking flame thickness into account. The median emissivity values obtained with Method 1 were represented against $\delta_{f_{rp}}$, whereas the emissivity values obtained with Method 2 were represented against the mean flame thickness (δ_{f_m}) because the entire flame, rather than one specific area, was studied with that method. Table 3 shows mean flame thickness values and standard deviations (SD). Note that SDs were higher for flame thickness values corresponding to Method 2. This variability was expected since the entire flame, from the base to the tip, was considered to compute an average flame thickness value. The data presented in Fig. 10 were fitted to a model equivalent to the one shown in Eq. (3). The extinction coefficient obtained from the Method 1 data had a value of 0.48 and an *R*-square value of 0.86, indicating satisfactory fitness. The extinction coefficient obtained from the Method 2 data had a value of 0.72 and an *R*-square value of 0.99, indicating very good fitness.

In the tests for which the fuel had previously been treated with a retardant product (EA ret1 and EA ret2), ignition was more difficult and the flames were narrower than those observed in the EA test, which was performed with the same fuel (*E. arborea*), but untreated (see Table 3). However, the emissivity values associated with these two tests followed the same trend as the data computed for the rest of the tests; this result was observed for both methods. Consequently, at the tested concentration level the retardant product did not modify flame emissivity and radiation continued being dominated by soot although ammonia, which is a major decomposition product of the retardant used in this study, has an absorbing band within the spectral range of the IR camera (at 10.5 μm) and the concentration of water vapour theoretically increased.

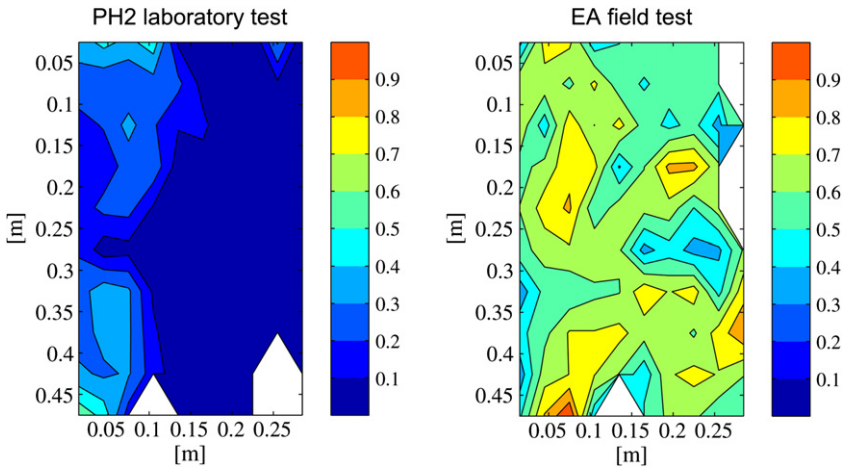

Fig. 8. Mean emissivity distribution for a laboratory test and a field test in the time domain used to compute emissivity by applying Method 1. White areas indicate unavailable data.

Fig. 11 shows flame emissivity data obtained by some of the authors mentioned in the review section (Section 2), as well as experimental data and exponential fit results obtained in this study by applying both methods. These data have been plotted against flame thickness (or, as in [22], against the side of the fuel bed). As in this study, data from the authors presented in Fig. 11 were fitted to exponential models to obtain extinction coefficient values. The only exception was the study by Dupuy et al. [17], because all of the data they obtained were in a very narrow range of flame thicknesses. They used a theoretical approach to obtain extinction coefficient values for soot.

The fitting results obtained in this study seem to correlate well with data obtained by Beyreis et al. [18]. These authors obtained an extinction coefficient of 0.51, which falls between the two values obtained here (0.48 for Method 1 and 0.72 for Method 2). High variability in values obtained by Beyreis et al. [18] may be due to the fact that maximum temperature values obtained with a unique thermocouple were employed to determine emissivity. Hägglund and Persson [16] obtained an extinction coefficient of 1.03, which is 43% higher than the one obtained in this study by applying Method 2. Differences between emissivity values determined by [16] and values obtained in this study may be due to several reasons, i.e. due

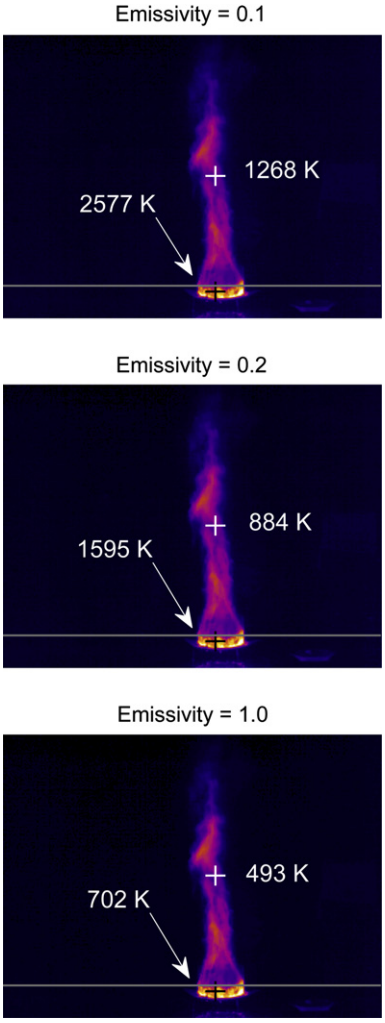

Fig. 9. IR image of the PH3 laboratory test considering three different emissivity values: 0.1, 0.2 and 1. Temperature values are shown for two fire pixels (i.e. flame and fuel bed pixels). The horizontal line divides the burning fuel bed from the flame.

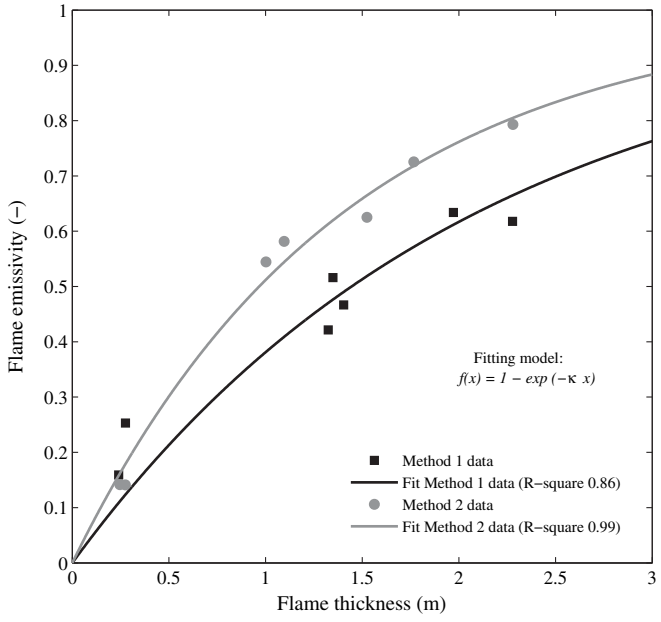

Fig. 10. Flame emissivity vs. flame thickness. Experimental data obtained in this study and exponential fit.

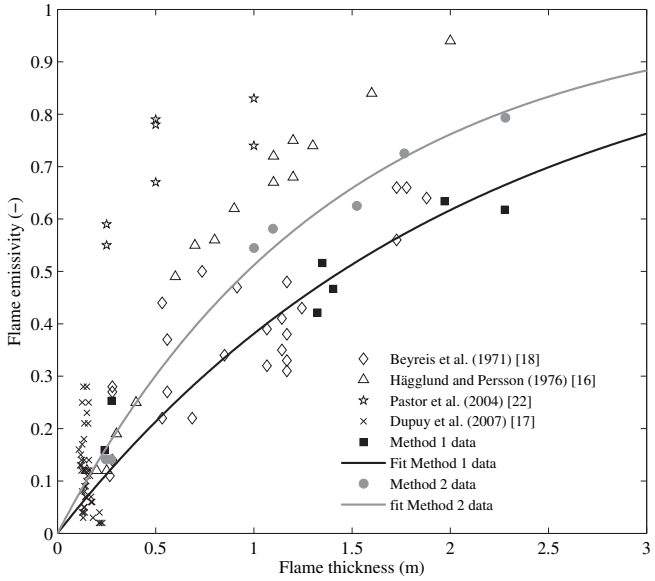

Fig. 11. Flame emissivity vs. flame thickness. Data obtained by other authors and data points and exponential fits for the data of this study.

to the fact that measurements were taken in different spectral ranges, due to the assumption taken in this study that flames were soot dominated or even due to the fact that flame emissivity values reported by [16] were highly dependent on flame temperature, a variable which is also very difficult to precisely determine when measured by thermocouples. The extinction coefficient obtained by Pastor et al. [22] was much higher than those calculated in this study (332% higher than the one obtained in this study by applying Method 2). This significant difference may be due to the fact that they used a blackbody that was at ambient temperature and radiation data from an IR camera working in the 623–1773 K temperature range. Measurements taken with and without the blackbody behind the flame were probably numerically similar, resulting in very high emissivity values. Experimental emissivity values obtained by Dupuy et al. [17] had a mean value of 0.11 and a relative standard deviation (RSD) of 63.6%. This high RSD is due to the fact that the authors computed emissivity values at different flame heights. Their mean emissivity value would fit the curves obtained in this study.

The two methods used in this study to compute flame emissivity can be compared in terms of type of results. For Method 1, the evolution of the emissivity can be observed at different points of the flame and the method itself is sensitive to the assumption of symmetry. Method 2 is easy to implement but can only obtain a mean emissivity value for the entire flame. The fitted model obtained from data extracted by applying Method 2 was better than the model fitted with data extracted by applying Method 1 (i.e. it had a higher *R*-square value). The extinction coefficient obtained by applying Method 1 was 33.3% smaller than the one obtained by applying Method 2. This difference may be explained by taking into consideration that the infrared camera used in this study was only sensitive to radiation in the spectral range from 7.5 to 13 μm, whereas the transducer measured total (including all wavelengths) heat flux. Flame emissivity values turned out to be higher with Method 2 to compensate for the energy contribution not sensed by the infrared camera. However, the difference between both extinction coefficients cannot be considered large, since theoretically this coefficient can take values from 0 to infinite, and values as high as 6.2 [17] have been reported for forest fuel flames.

According to the results obtained in this study, flame emissivity values close to that of a blackbody (0.90) are only attained for flame thicknesses of 4.8 m and 3.2 m for Method 1 and Method 2, respectively. These results contradict the conclusion of Hägglund and Persson [16], who determined that 2-m-thick forest fuel flames had an emissivity in excess of 0.9. However, they are in agreement with the results of Beyreis et al. [18], who found an emissivity of 0.9 for a flame thickness of 4.5 m.

6. Conclusions

The concept of flame emissivity is usually employed to solve radiative heat transfer problems in forest fires propagation. To characterize the emission of flames a kind of equivalent medium assumption has to be made since flame emission is produced by a varying semitransparent volume.

In this study, the experimental methods developed to date to compute the emissivity of forest fuel flames were reviewed. Two particular methods were developed to compute emissivity values from flames generated during the combustion of branches and leaves of typical Mediterranean forest fuels. One of these two methods (Method 2) represents an improvement of the approach used by Thomas [19], since it differentiates between the two radiating sources of the fire (flame and burning fuel bed). The other method (Method 1) represents a modification in terms of set-up of the flame transmission method also used in [17,21,22]. An IR camera sensitive at the spectral range from 7.5 to 13 μm was used to apply both methods. Several assumptions had to be made to apply and compare both methods, such as a grey medium assumption for sooty flames and homogeneity for the equivalent medium representing the flames.

The emissivity values obtained here were exponentially correlated against flame thickness. Two different extinction coefficients were obtained: 0.48 for Method 1 and 0.72 for Method 2. Despite this difference, both sets of data showed the same trend as the experimental values of Beyreis et al. [18], who obtained flame emissivity values by using a methodology not dependent on the spectral range of measurement. According to our results, flames thicker than 3.2 m would exhibit an emissivity value close to that of a blackbody (0.9). Moreover, the emissivity of the flame was unaffected by the presence of a long-term retardant product in the fuel at a concentration level of 0.75 l of dilution (15% V/V) per kg of fuel.

Acknowledgments

This study was supported by the Spanish Ministry of Education and Science as part of project AGL2005-07269. It was also supported by the Commission for Universities and Research of the Ministry of Innovation, Universities and Enterprise of the Catalan Government, the European Social Fund and the Universitat Politècnica de Catalunya (UPC). The authors would like to acknowledge the comments made by the reviewers, which contribute to improve the paper.

References

[1] F.A. Albini, A model for fire spread in wildland fuels by radiation. Combust. Sci. Technol. 42 (1985) 229–258. doi:10.1080/00102208508960381.
[2] D. Morvan, J.-L. Dupuy, Modeling of fire spread through a forest fuel bed using a multiphase formulation. Combust. Flame 127 (2001) 1981–1994. doi:10.1016/S0010-2180(01)00302-9.
[3] N.J. De Mestre, E.A. Catchpole, D.H. Anderson, R.C. Rothermel, Uniform propagation of a planar fire front without wind. Combust. Sci. Technol. 65 (1989) 231–244. doi:10.1080/00102208908924051.
[4] R.R. Linn, A transport model for prediction of wildfire behavior, PhD thesis, New Mexico State University, USA, 1997. Also published as Los Alamos National Laboratory Report number LA-13334-T.
[5] A. Simeoni, P.-A. Santoni, M. Larini, J.-H. Balbi, Reduction of a multiphase formulation to include a simplified flow in a semi-physical model of fire

spread across a fuel bed. Int. J. Therm. Sci. 42 (2003) 95–105. doi:10.1016/S1290-0729(02)00009-1.
[6] D. Morvan, J.-L. Dupuy, Modeling the propagation of a wildfire through a Mediterranean shrub using a multiphase formulation. Combust. Flame 138 (2004) 199–210. doi:10.1016/j.combustflame.2004.05.001.
[7] A.L. Sullivan, P.F. Ellis, I.K. Knight, A review of radiant heat flux models used in bushfire applications. Int. J. Wildland Fire 12 (2003) 101–110. doi:10.1071/WF02052.
[8] B. Portiere, D. Morvan, M. Larini, J.C. Loraud, Wildfire propagation: a two-dimensional multiphase approach. Combust. Explo. Shock Waves 34 (1998) 139–150. doi:10.1007/BF02672813.
[9] W.R. Catchpole, E.A. Catchpole, The second generation US firespread model. Final report of RMRS-94962-RJVA, 2000. Joint research venture of the US Forest Service and ADFA.
[10] A. Pappa, K. Mikedi, N. Tzamtzis, M. Statheropoulos, Chemometric methods for studying the effects of chemicals on cellulose pyrolysis by thermogravimetry–mass spectrometry. J. Anal. Appl. Pyrolysis 67 (2003) 221–235. doi:10.1016/S0165-2370(02)00063-3.
[11] N. Tzamtzis, S. Karma, A. Pappa, M. Statheropoulos, On-line monitoring of pine needles combustion emissions in the presence of fire retardant using a 'thermogravimetry (TG)-bridge/mass spectrometry method'. Anal. Chim. Acta (2006) 573–574. doi:10.1016/j.aca.2006.05.047 439–444.
[12] N.K. King, The influence of water vapour on the emission spectra of flames. Combust. Sci. Technol. 6 (1973) 247–256 doi:10.1080/00102207308952327.
[13] R. Siegel, J.R. Howell, Fundamentals and properties for radiation in absorbing, emitting, and scattering media. in: M. Prescott, C.V. Ormes (Eds.), Thermal Radiation Heat Transfer, third ed. Taylor and Francis, USA, 1992.
[14] T. Sato, T. Kunimoto, S. Yoshi, T. Hashimoto, On the monochromatic distribution of the radiation from the luminous flame. Bull. Jpn. Soc. Mech. Eng. 12 (1969) 1135–1143.
[15] D. Drysdale, An Introduction to Fire Dynamics. John Wiley & Sons Ltd., New York, 1997.
[16] B. Hägglund, L.-E. Persson, An Experimental Study of the Radiation from Wood Flames. Försvarets Forskningsanstalt Huvudenhet, FoU-brand, Stockholm, 1974.
[17] J.-L. Dupuy, P. Vachet, J. Maréchal, J. Meléndez, Thermal infrared emission-transmission measurements in flames from a cylindrical forest fuel burner. Int. J. Wildland Fire 16 (2007) 324–340. doi:10.1071/WF06043.
[18] J.R. Beyreis, H.W. Monsen, A.F. Abbasi, Properties of wood crib flames. Fire Technol. 7 (1971) 145–155 doi:10.1007/BF02588954.
[19] P.H. Thomas, Rates of spread of some wind-driven fires. Forestry 44 (1971) 155–175. doi:10.1093/forestry/44.2.155.
[20] I.K. Knight, A.L. Sullivan, A semi-transparent model of bushfire flames to predict radiant heat flux. Int. J. Wildland Fire 13 (2004) 201–207. doi:10.1071/WF03047.
[21] E. Den Breejen, M. Roos, K. Schutte, J.S. De Vries, H. Winkel, Infrared measurements of energy release and flame temperatures of forest fires. in: D.X. Viegas (Ed.), Proceedings of the 3rd Int. Conf. on Forest Fire Research (Luso-Coimbra, 1998). Associação para o Desenvolvimento da Aerodinâmica Industrial (ADAI), Coimbra, Portugal, 1998, pp. 517–532.
[22] E. Pastor, A. Rigueiro, L. Zárate, A. Giménez, J. Arnaldos, E. Planas, Experimental methodology for characterizing flame emissivity of small scale forest fires using infrared thermography techniques. in: D.X. Viegas (Ed.), Proceedings of the 4th Int. Conf. on Forest Fire Research (Luso-Coimbra, 2002). Millpress, Rotterdam, Netherlands, 2002 CD-Rom.
[23] R. Vélez (coordinator), Medios y métodos para la modificación de los combustibles. In: A.G. Grace (Ed.), La Defensa contra Incendios Forestales. McGraw-Hill, Madrid, 2000.
[24] H.E. Anderson, Aids to Determining Fuel Models for Estimating Fire Behaviour. USDA Forest Service, Intermountain Forest and Range Experiment Station Odgen, 1982, General Technical Report INT-122.
[25] C. Qian, K. Saito, Measurements of pool-fire temperature using IR technique. in: J.P. Gore (Ed.), Proceedings of Combustion Fundamentals and Applications (Joint Technical Meeting), San Antonio, TX, USA (1995), pp. 81–86.
[26] M. Muñoz, Estudio de los parámetros que intervienen en la modelización de los efectos de grandes incendios de hidrocarburo: geometría y radiación térmica de la llama, PhD thesis, Universitat Politècnica de Catalunya, Spain, 2005.
[27] Toolkit IC2 Dig 16, Developers Guide 1.00 AGEMA 550/570 (AGEMA file format) file description; FLIR Systems AB Publication number: 557 344 version B.
[28] H.P. Telisin, Flame radiation as a mechanism of fire spread in forests. in: N.H. Afgan, J.M. Beer (Eds.), Heat Transfer in Flames. John Wiley & Sons Ltd., New York, 1974.
[29] R.C. Corlett, Velocity distribution in fires. in: P.L. Blackshear (Ed.), Heat Transfer in Fires. John Wiley & Sons Ltd., New York, 1974.